LIVERSIDGE LECTURE. The Dynamics of Photodissociation

Richard N. Dixon
School of Chemistry, University of Bristol, Bristol BS8 ITS, U.K.

1 Introduction

A major object of modern chemical physics has been to obtain a detailed understanding of the factors that control chemical reaction dynamics, with the eventual goal of designing reactions to have a predetermined outcome. This is a field in which there has been a particularly strong interplay between ongoing experimentation and parallel theoretical developments. Molecular beams and lasers have been instrumental in many recent advances, most particularly in the study of photodissociation. This is inherently one of the simpler types of reaction in that the products are already in close contact in the reactant, and its detailed study has greatly advanced our theoretical understanding of reaction dynamics. These advances have highlighted two extremes for the distribution of the available energy over product motion; namely, those cases where the energy becomes statistically distributed over all possible product states, and those exhibiting specific dynamical control.

Photochemically initiated reactions are of course also of intrinsic importance to us in such diverse ways as the generation of the ozone layer in the upper atmosphere which protects us from ultraviolet irradiation; in the photosynthetic cycles which provide much of our food; and in the recording of information by photographic means.

Early photochemical experiments were initiated using flash lamps, which usually give out a range of photon energies. While such experiments often led to the identification of the reaction pathways and the detection of unstable intermediates, they did not necessarily reveal the detailed motion during the primary bond-breaking step. The use of lasers, and particularly tuneable dye-lasers, both to initiate photochemical decomposition and to probe the identity of, and energy disposal within, the primary reaction products, has removed this limitation.

These advances are a consequence of four properties of lasers: monochromaticity, which often permits parent molecule activation and product detection at a quantum specific level; intensity, which enhances the sensitivity of product detection, permitting low enough pressures in the gas phase to avoid collisional relaxation, and also facilitates multiphoton excitation to high energy states; directionality and polarization, which can be used to probe the correlation between the vectorial properties of the transition dipoles and the rotational or translational motions of the products, thereby giving insight into the stereo-specificity of the primary reaction step; and pulse duration, which at its shortest can match the femtosecond time-scale of the motions of the atoms in a molecule.

Diatomic molecules have the most simple dynamics of photodissociation because the (one) vibrational coordinate is also the reaction coordinate (Figure 1). When a diatomic molecule is excited by absorption of a photon to an electronic state having a potential energy curve repulsive between the atoms they will recoil from one another on the time-scale of a vibrational period ($\sim$ 30 fs). This is termed *direct dissociation*, and is characterized by a structureless absorption spectrum for the parent molecule (recall the Uncertainty Principle). In contrast, a highly struc-

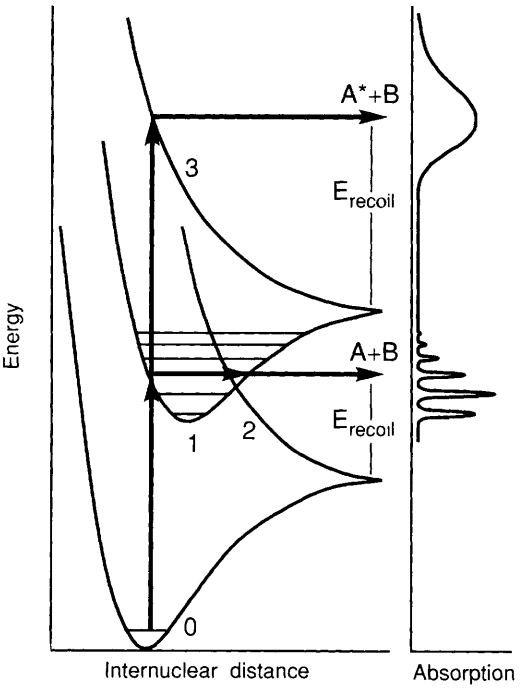

Figure 1 Schematic representation of potential curves and the corresponding absorption spectra for a diatomic molecule AB. Electronic state 1 is bound, but its levels are predissociated through interaction with the continuum of state 2. The absorption from state 0 to state 1 therefore consists of broadened lines, with widths inversely proportional to the dissociation lifetime. Electronic state 3 is directly dissociative, and the absorption spectrum from state 0 to state 3 consists of a broad continuum.

Richard Dixon is the Alfred Capper Pass Professor of Chemistry at the University of Bristol. He was educated at the Judd School, Tonbridge, at King's College, London, and at St. Catharine's College, Cambridge. His interest in spectroscopy was kindled by W. C. Price at King's, where he graduated with first class honours in physics.

A desire to move to chemistry led to a Ph.D. in infrared spectroscopy under N. Sheppard at Cambridge. He spent two years as an analyst with the Atomic Energy Authority. This was followed by three postdoctoral years in Canada. Returning to England, he spent one year as an ICI fellow and nine years as a lecturer in chemistry at Sheffield University. He was the Sorby research fellow of the Royal Society for the last five of these years. He was appointed to the chair of theoretical chemistry at Bristol University in 1969, and the Capper Pass chair in 1990.

Dixon's early spectroscopic research was concerned principally with molecular structure, initially of stable molecules but then increasingly of transient species. This broadened into an interest in photochemistry and time-dependent molecular phenomena. His experimental studies have been underpinned by the development of theoretical models of molecular structure and quantum dynamics. Previous recognition includes the RSC Corday-Morgan medal (1966) and the spectroscopy award (1984). He was elected to the fellowship of the Royal Society in 1986.

tured absorption spectrum indicates the presence of a potential well for the excited state, giving rise to long-lived states which may often be characterized by excited state quantum numbers. Any dissociation from these states occurs on a slower time-scale than for direct dissociation. This is termed *predissociation*, and is brought about by quantum tunnelling through a barrier, or by a change of electronic state near a curve crossing. In either case, any excess energy above the electronic energy of the separated atoms (the available energy) must appear in their mutual recoil:

$$E_{\text{parent}} + h\nu - E_{\text{atoms}} \equiv E_{\text{available}} \rightarrow E_{\text{recoil}} \quad (1)$$

Polyatomic molecules have a much richer diversity of dissociation mechanisms, since energy can flow between many internal modes of excitation, and the distinction between direct and indirect dissociation is less clear-cut than in diatomic molecules. In his classic book Herzberg[1] classified polyatomic predissociation mechanisms into case I, predissociation by electronic transition; case II, predissociation by vibration; and case III, predissociation by rotation. It is now recognized that it is possible for these processes to occur simultaneously with rates that may vary with the vibrational or rotational quantum numbers, giving a quantum state specificity to the mechanism.

Energy flow between internal modes during dissociation is not limited to long-lived states. In direct dissociation of a polyatomic molecule into fragments X and Y the potential will be repulsive along the coordinate R_{XY} between the centres of mass of the fragments X and Y, thereby promoting recoil. But the structures of minimum energy for X and Y in the parent molecule may differ from those in the isolated fragments after dissociation, or the atoms initially connected by the breaking bond may be dynamically coupled to the vibrational modes within X and Y. In either case the motion of the atoms during dissociation is not simply one of extension of R_{XY}, and part of the available energy ends up as internal excitation of either product instead of mutual recoil:

$$E(\text{X–Y}) + h\nu - E_{\text{dissociation}} \rightarrow E_{\text{internal}}(\text{X}) + E_{\text{internal}}(\text{Y}) + E_{\text{recoil}}(\text{X} \leftrightarrow \text{Y}) \quad (2)$$

In an ideal experiment the distribution of motion between all these degrees of freedom would be determined in full, albeit with some redundancy through conservation laws. The internal energies of the fragments are usually probed using laser-induced fluorescence (LIF) or resonance-enhanced multi-photon ionization (REMPI) spectroscopy, with relative populations obtained *via* line intensities. The distribution of recoil velocities is measured through the Doppler-broadening of lines in the LIF or REMPI excitation spectra, or with higher resolution by free time-of-flight (TOF) over a known pathlength using electron bombardment ionization or REMPI with detection *via* ions.

In molecules with no more than about six atoms good quality potential energy surfaces may be available through quantum chemical calculations. Where known, these have provided a valuable framework with which to interpret photochemical experiments, particularly when the time-dependent nuclear Schrödinger equation is used to calculate the nuclear motion on a single excited surface. However, many dissociation products are open-shell species, and when two such entities are brought together several potential surfaces of the combined system correlate with each dissociation limit. The consequence is that there are usually many surface crossings in polyatomic molecules, and the different channels may even lead to different chemical products, such as $H_2O^* \rightarrow H + OH$ or $H_2 + O$.

This article summarizes recent advances in photodissociation, with particular emphasis on systems with which the author has been involved. The molecular systems are grouped according to their basic mechanisms. Section 2 covers dissociation on a single potential energy surface: Section 3 dissociation mediated by a crossing of potential energy surfaces; and Section 4 dissociation following internal conversion to the vibrational continuum of the molecular ground state. Section 5 summarizes ongoing developments.

2 Dissociation on a Single Potential Energy Surface

Where dissociation takes place on a single potential energy surface the Born–Oppenheimer separation of electronic and nuclear motion is usually valid. It is then sufficient to consider the dynamics of the nuclear motion independently of that of the electrons, although there may be some recoupling of electron spin or orbital motion as the products are formed at long range. This is the case in each of the examples given below. A quantitatively accurate theoretical description of the dynamics requires a quantum treatment, but a swarm of classical trajectories with starting conditions that mimic the distribution of positions and momenta of a Franck–Condon wavepacket is equally informative.

2.1 H_2O $\tilde{A}$ State

A simple example of a direct dissociation is provided by the dissociation of water vapour excited in its first ($\tilde{A}\,^1B_1$–$\tilde{X}\,^1A_1$) electronic absorption band near 165 nm,[2] in that most of the available energy appears as mutual recoil of H from OH (Table 1).

Table 1 The distribution of the available energy for photolysis of H_2O at 157 nm

Fraction in translational recoil	f_t	~ 90%
Fraction in OH rotation	f_r	~ 1.2%
Fraction in OH vibration	f_v	~ 10%

When the H_2O is jet cooled to *ca.* 10 K only about 240 cm^{-1} appears as OH rotational energy. This modest rotation derives largely from the zero-point energy of the H_2O bending vibration ν_2 which is a disappearing mode. The two H atoms share most of the initial HOH bending kinetic energy of $\nu_2/4 \sim 415\ cm^{-1}$ in the form of relative angular oscillations of the bonds. Upon photolysis this correlates with tangential motion of one H atom and rotation of its OH partner, thereby imparting an average of ~ 210 cm^{-1} of rotational energy to the OH fragment.

Two points of note in this system are: (i) with excitation by linearly polarized light the axis of OH rotation is strongly aligned parallel to the electric field. Since the transition moment for $^1B_1$–$^1A_1$ is perpendicular to the H_2O plane, the sense of this alignment confirms that the rotational motion takes place in the instantaneous plane of the parent molecule; (ii) one set of Λ-doublets of the OH ($X^2\Pi$) radical product is much more strongly populated than the other, indicating that the unpaired electron left behind in OH is strongly constrained to lie in a $2p\pi$ orbital perpendicular to this plane of rotation. This is a clear example of an orbital conservation rule: one electron in water is excited from a $2p\pi$ lone-pair orbital to an in-plane anti-bonding orbital, and goes away on the departing H atom, leaving its unpaired partner behind in the $2p\pi$ orbital of the rotating OH molecule:

$$\begin{aligned} H_2O\,(\cdots, 2pa_1^2, 2pb_1, 3s\sigma^*a_1; \tilde{A}\,^1B_1) \rightarrow H(1sa'; {}^2S) \\ + OH(\cdots, 2p\pi a'^2, 2p\pi a''; X^2\Pi'') \end{aligned} \quad (3)$$

Considerably more energy appears as OH vibration, with population in $v = 0,1$, and 2. Dynamical calculations on an *ab initio* potential surface have shown that to a considerable degree this excitation has its origin in the symmetry of H_2O. Excitation at the ground-state geometry (a vertical transition in accordance with the Franck–Condon principle) leads to a region of the upper-state potential where its slope results in an initial repul-

sion along the symmetric bond-stretching coordinate. However, at longer range there is a high barrier inhibiting dissociation along this coordinate because this would require both bonds to break. A small probability of vibration back to the Franck–Condon region gives rise to the observed slight undulations on the absorption band profile, with a vibrational spacing of $\sim 1900\ cm^{-1}$, but in general this barrier deflects the motion towards stretching of only one bond. Even so, some of the initial symmetric excitation remains as vibration of the unbroken OH bond as the H and OH move apart, the extent of which increases with increase in the available energy.

2.2 H_2O_2 $\tilde{A}$ State

The direct association of hydrogen peroxide is strikingly different. Photolysis within its first continuum ($\tilde{A}^1A$–$\tilde{X}^1A$) at 266 or 248 nm releases about 11% of the available energy into OH rotation but gives no vibrational excitation.[3] However, the novel feature revealed by a polarization study of OH Doppler line profiles[4] is the opposite signs of the effective recoil anisotropy parameters β_{eff} for related pairs of transitions when recorded with the detection geometry of Figure 2. This indicates that there is a strong correlation between the fragment rotational and translational vectors J_{OH} and v_{OH}, with a clear preference for rotation *around* the axis of recoil. This non-trivial result cannot be the result of initial zero-point energy of disappearing bending vibrations, but is the dynamical consequence of forces that act during the dissociation.

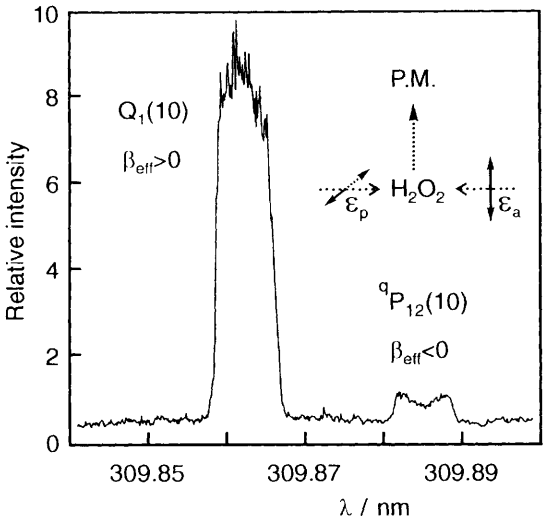

Figure 2 Line profiles, Doppler-broadened by the recoil velocity v, in the LIF excitation spectrum of the OH fragments from photolysis of H_2O_2 at 266 nm. The photolysis (polarization axis ϵ_p) and analysis (polarization axis ϵ_a) laser beams were counter-propagated, and the fluorescence was detected with a photomultiplier (P.M.) at right angles. The two transitions have the same lower level, and thus probe the same group of molecules, but with opposite angular anisotropy relative to the axes of their rotational angular momentum J. The contrasting profiles show that v and J have a parallel correlation.

Repulsion between lone-pair electrons on the two O atoms bestows a skewed equilibrium structure to H_2O_2 in its ground state, with a dihedral angle of $\sim 111.5°$ between the two OH bonds. The lowest energy electronic transition involves the promotion of one of these lone-pair electrons to an anti-bonding orbital, as in H_2O. This excitation generates repulsion between the O atoms, resulting in HO↔OH recoil, but it also removes the twisting force so that the initial motion is for the H atoms to move towards planarity as the fragments move apart. The result of this torque is that the OH radicals recoil in a corkscrew fashion, with much greater excitation of rotational motion than in OH from H_2O (Figure 3). These dynamics appear to be a

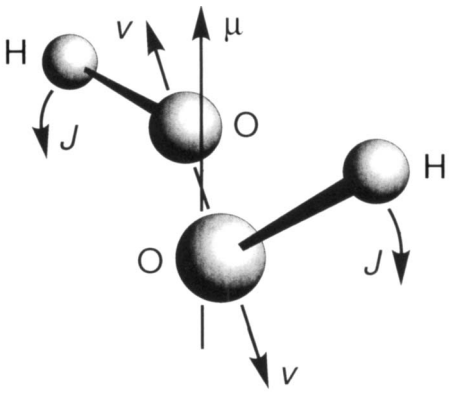

Figure 3 The dynamics of the dissociation of H_2O_2 following excitation in its first absorption band, for which the transition dipole μ bisects the angle between the two OH bonds. The H atoms move towards a trans-planar geometry as the OH radicals start to separate. Thus both the recoil velocities v and the most probable OH rotational vectors J are perpendicular to the dipole axis and parallel to each other.

general characteristic of the peroxide bond, and a very similar behaviour has been found for the OH fragment from heavier peroxides such as tertiary butyl peroxide.

2.3 HONO $\tilde{A}$ State

Nitrous acid, HONO, provides a good example of a molecule with an excited state which is sufficiently long-lived to permit transient vibration. The near ultraviolet absorption spectra of nitrous acid, and of all alkyl nitrites, show diffuse overlapping bands with a mean spacing of $\nu_2' \sim 1100\ cm^{-1}$ characteristic of the vibration of a weak terminal NO bond. Dissociation to give the two molecular products (OH and NO) is mediated by a partial energy-transfer between the vibration of this terminal bond and stretching of the central bond. The Doppler widths of the lines in the spectra of both products show that about two thirds of the available energy is liberated in their mutual recoil.

Dissociation of HONO at 355 nm, which is the most studied wavelength, proceeds *via* the 2_0^1 band (excitation to the quasi-bound level with $v_2' = 2$). This yields OH exclusively in its ground vibrational level, with little rotational excitation ($E_{rot} \sim 210\ cm^{-1}$). In contrast the vibrational levels of NO are populated up to $v = 3$, each with a high and inverted rotational excitation (Table 2). The OH line profiles, together with momentum conservation, show that $f_t \sim 60\%$ for the combined OH and NO recoil fraction of the energy, and that all the available energy has been accounted for.[5,6]

Table 2 The distribution of the available energy for photolysis of HONO at 355 nm

Fragment molecule		OH	NO
Fraction in translational recoil	f_t	38%	22%
Fraction in rotation	f_r	2%	13%
Fraction in vibration	f_v	~0%	25%
Electronic orbital alignment	$\Pi(A'')$:$\Pi(A')$	1:3.4	2.8:1

Polarization studies confirm that the rotational motions of both the OH and NO fragments are largely constrained to the original HONO plane. The observed Λ-doublet propensities (Table 2) show that an in-plane π-orbital ($\pi a'$) is favoured for the unpaired electron of the OH, but an out-of-plane π-orbital ($\pi a''$) for the NO electron. This is consistent with an electronic rearrangement in which the central N–O σ-bond is broken following an out-of-plane π^*–n excitation within the –NO group (Figure 4).

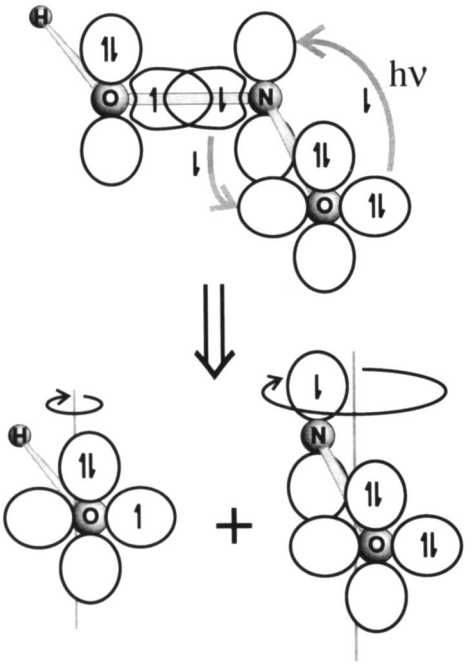

Figure 4 Electronic rearrangements during the photolysis of nitrous acid. The π^*–n excitation weakens both the HO–NO and HON–O bonds. Stretching of the central bond is then associated with a back transfer between in-plane orbitals, restoring the strength of the terminal NO bond (see the potential contours of Figure 6), leaving one unpaired electron on each rotating fragment with the indicated stereospecificities.

As in the case of H_2O discussed above, the modest rotation of the OH fragment derives from disappearing bending modes, of which the in-plane ∠HON vibration has the highest frequency. In contrast, the NO rotation is far too energetic for such an origin (Figure 5). The contrasting patterns of OH and NO rotational excitation are readily understood if much of the available energy is released in repulsion directed between the central O and N atoms. A force along this bond passes close to the centre of mass of OH, but exerts a strong torque around the more distant centre of mass of NO. Thus a significant fraction of this repulsive energy release will be channelled into NO rotation, but very little into OH rotation. Model calculations show that the NO rotational excitation is slightly less than predicted by this simple impulse picture.

The explanation of the vibrational branching has been guided by *ab initio* calculation of the potential energy surface, and is illustrated by classical trajectories in Figure 6 (note that the complete mechanism involves synchronous oscillation of the ∠ONO angle as well as stretching motions). We can consider this dissociation to occur in two steps. In the first slow step ($\tau \leq 90$ fs) V–V transfer partially redistributes the excitation energy between vibration along the (HO)N–O and (H)O–N(O) coordinates until the motion is directed towards a well-defined saddle point. Most of the available energy is then released impulsively in a fast second-step during which there is little change in the vibrational distribution of the emerging NO, and the motion is largely confined to a plane thereby generating the translational recoil and NO rotation. The dissociation of alkyl nitrites follows a similar pattern, albeit with some vibrational excitation of the alkyl radicals. This family therefore typifies Herzberg's predissociation by vibration (case II). The essential feature which gives rise to this behaviour is the rapid change in bonding as the central ON bond is stretched. This results in the shallow potential minimum which can support transient vibration, with dissociation driven by the anharmonicity of this potential.

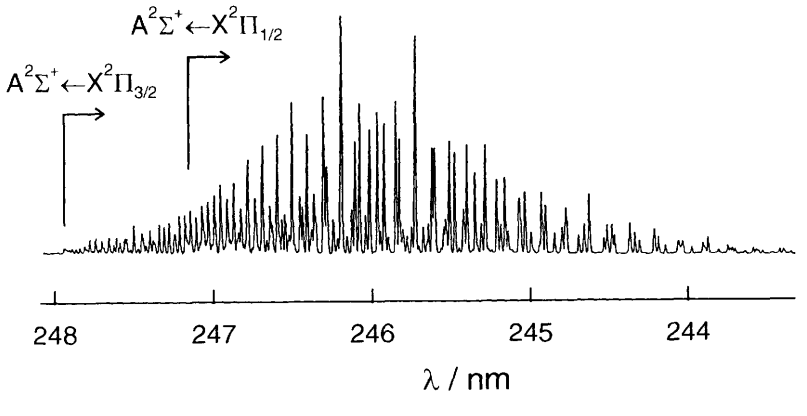

Figure 5 The LIF excitation spectrum of the NO(A–X) 0–2 band following photolysis of HONO at 355 nm. The profile of this band reflects the population distribution within the $v'' = 2$ lower state. This is approximately Gaussian in rotational quantum number, with a mean value of $J_m = 26$ and a standard deviation of $\sigma_J = 6.5$.

3 Dissociation Mediated by Surface Crossings

There are three common types of surface crossing for which symmetry plays an important role. In molecules such as H_2O, HCO, and SiF_2^+ there are states which are orbitally degenerate for a linear geometry, but this degeneracy is lifted by bending

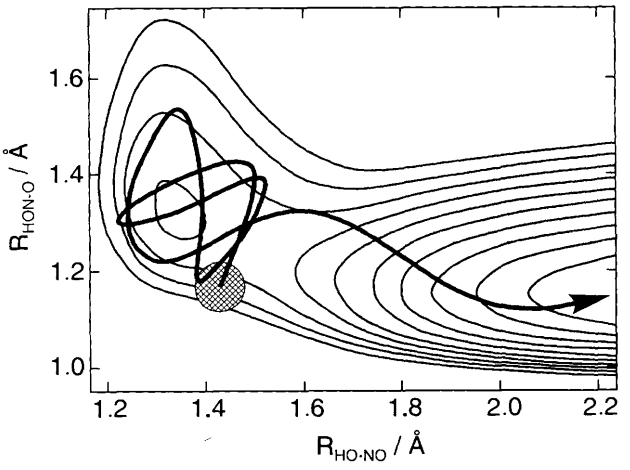

Figure 6 A representative trajectory showing the relative motions in the ON and NO coordinates of HONO during photodissociation. The initial motion starts in the Franck–Condon region of coordinates (hatched), and is principally a vibration of the terminal NO bond. However, part of the vibrational energy becomes redistributed into motion of the central ON bond, thereby facilitating escape from the shallow potential well.

with a splitting which initially increases quadratically with the amplitude of bending The two component states have different symmetry in the lower point group, and can only be mixed through electronic Coriolis interactions in a rotating molecule (the Renner–Teller effect) In the second type, for molecules such as H_2S or NH_3, two independent surfaces of different character cross in configurations of high symmetry, but have the same character on distortion to a lower point group This results in a 'conical intersection' of the potential hypersurfaces in which the splitting between them is initially linear in two or more nuclear coordinates Finally, for molecules such as CH_4, there is a conical intersection which derives from an orbital degeneracy in a non-linear configuration of high symmetry (the Jahn–Teller effect) In both these latter cases the interstate coupling is vibronic in origin and is independent of rotation

The examples below illustrate each of these types of surface intersection We will see that there are cases where a surface is subject to more than one of these crossing mechanisms

3.1 The $\tilde{A}^2A''$ and $\tilde{X}^2A'$ States of HCO

The emission spectrum known as the 'hydrocarbon flame bands', which has also recently been observed in LIF, provides experimental data for a large number of vibrational levels of HCO in its electronic ground-state [7] Many of these bands show a rotational diffuseness which arises from the predissociation of those lower levels which lie above the dissociation limit for HCO ($\tilde{X}^2A'$) → H + CO ($X^1\Sigma^+$) This is another example of Herzberg's predissociation by vibration (case II) These levels will not be discussed further save to note that their resonance energies and widths are well accounted for by a three-dimensional time-dependent wavepacket calculation using an *ab initio* potential energy surface The widths show systematic trends with increases in the vibrational quantum numbers, but not simply with the level energies [8]

The $\tilde{A}^2A''$ state also has a structure of predissociated vibronic levels The longest-lived excited levels are those with $K_a = 0$, and the dissociation rate increases with increase in K_a and decreases with increase in v_2' (Figure 7) This is in quantitative accord with a model calculation[9] for a Renner–Teller (Coriolis) induced coupling to the ground-state continuum (Figure 8), in keeping with the knowledge that this excited state has the wrong symmetry to correlate adiabatically with ground-state products which are the only ones energetically accessible

A second more surprising consequence of the Coriolis nature of this surface crossing concerns the observed recoil anisotropy of both the H(D) and CO dissociation products from HCO and from DCO [10] The $\tilde{A}^2A'' \rightarrow \tilde{X}^2A'$ transition moment is perpendicular to the HCO plane It would therefore be anticipated that

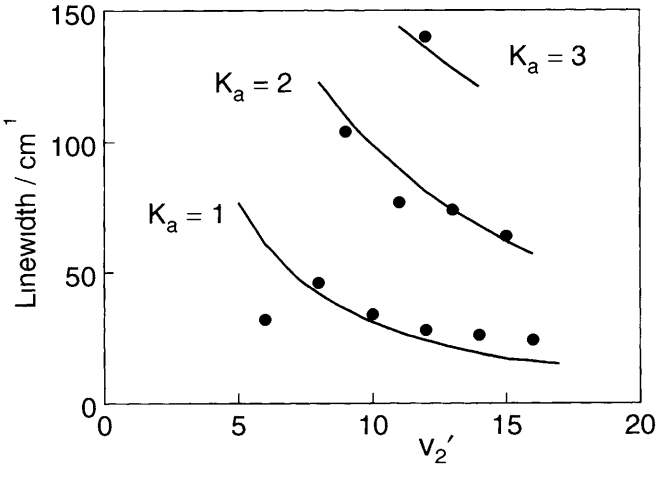

Figure 7 The variation with the quantum numbers for bending (v_2') and a-axis rotation (K_a) of the linewidths in the $\tilde{A}^2A''$ excited state of HCO ● experimental values, —— calculation

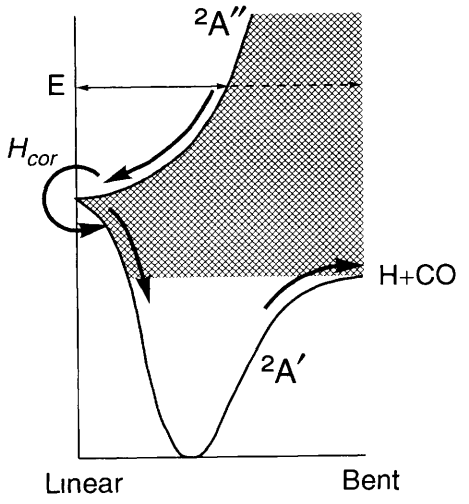

Figure 8 The dissociation of a quasi-bound vibrational level of the $\tilde{A}^2A''$ state of HCO at energy E by coupling to the continuum of the $\tilde{X}^2A'$ ground state (hatched) The surface-crossing is mediated by electron–nuclear Coriolis forces in near linear HCO The bold arrows indicate the variation of the electronic energy along the dissociation path

recoil would take place preferentially in a plane perpendicular to the axis of the electric vector of a linearly-polarized photolysis laser, leading to a negative recoil anisotropy parameter β In fact β is found to vary with the vibronic band chosen for excitation, but is either zero or positive, the largest values being between 0 7 and 1 0 This is best explained in terms of a simplified representation of the stationary state wavefunctions for the coupled states, in which we consider explicitly only the rotation about the molecular a-axis

Let Λ [= 1 for HCO $\tilde{A}/\tilde{X}^2\Pi_u$], conjugate to the body-fixed electronic angle α, and K, conjugate to the a-axis rotational angle ϕ, be good quantum numbers let θ be the ∠HCO angle, r the CO bond-length, and R the H–CO dissociation coordinate The greatest recoil anisotropy is found to be for excitation *via* the $K' = 1 \leftarrow K'' = 0$ sub-bands (Table 3) For these, with $\phi = 0$ defined by the axis of the laser polarization, the two-component wavefunction for the excited state K doublet is

$$\psi_{i\,K^+} = \pi^{-1}\psi_e(r_e)\left[u^A_{iK}(\theta, r, R)\sin(\Lambda\alpha)\sin(K\phi) - u^A_{iK}(\theta, r, R)\cos(\Lambda\alpha)\cos(K\phi)\right] \quad (4)$$

In this equation the $\tilde{A}$ and $\tilde{X}$ Born–Oppenheimer states are assumed to have a common electronic wavefunction $\psi_e(r_e)$ in all coordinates except the angle α, and the u functions are vibrational wavefunctions associated with these two surfaces The excitation transition moment from the ground-state couples to the first ($\tilde{A}^2A''$) term, which has the major amplitude For K = 1 this peaks at $\phi = 90°$ as expected for this perpendicular transition Even so, only the second ($\tilde{X}^2A'$) term with the minor amplitude $u^A(\theta, r, R)$ extends out to dissociation at $R = \infty$, and this component peaks at $\phi = 0$ leading to a positive value for β Table 3 presents the comparison between the observed values of

Table 3 A comparison of the observed and calculated recoil anisotropy parameter β for HCO (DCO) $\tilde{A}^2A'' \rightarrow H(D) + COX^1\Sigma^+$

K′	sub-band	β observed	β calculated
0^-	$0 \leftarrow 1(Q)$	0 25	0 13
0^-	$0 \leftarrow 1(R)$	0 0	−0 06
1^+	$1 \leftarrow 0$	0 7—1 0	1 04
$1^+, 1^-$	$1 \leftarrow 2$	0 0	0 08
$2^+, 2^-$	$2 \leftarrow 1$	0 1—0 15	0 12

β and those calculated with wavefunctions such as in equation 4, with the further assumptions that the H atom departs at 60° to the a-axis which is the minimum energy path to dissociation on the ground-state surface, and with allowance for some degradation of β through end-over-end rotation of the HCO.[10]

Thus this unusual recoil anisotropy comes about because of the need for the electrons and nuclei to transiently exchange angular momentum in order to facilitate the non-adiabatic surface crossing at linearity. For the $K' = 1 \leftarrow K'' = 0$ sub-bands the most probable plane of dissociation is at right angles to that of excitation.

The two-component wavefunction of equation 4 also leads to an understanding of the energy distribution among the vibrational and rotational levels of the CO photofragment.[11] In a time-dependent view of dissociation from the $\tilde{A}$ state of HCO, the early motion of a wavepacket representing the vertical excitation from $\tilde{X}$ to $\tilde{A}$ (the first component in equation 4) will be towards linearity, as indicated in Figure 8. The Coriolis coupling will then generate the second component on the ground-state surface. In three dimensions this second component will initially be tightly constrained around a saddle-point as indicated in Figure 9, but will then follow a bending trajectory towards the energy minimum. This figure presents a two-dimensional cut of such a three-dimensional second-component wavefunction 15.9fs after crossing from the $\tilde{A}$-state surface, calculated using the *ab initio* $\tilde{X}$-state surface. By this time the wavepacket has bounced off a steep repulsive wall on the surface; part has been reflected back towards the linear saddle-point, and part has been deflected out towards dissociation over a region of the potential which is almost flat.

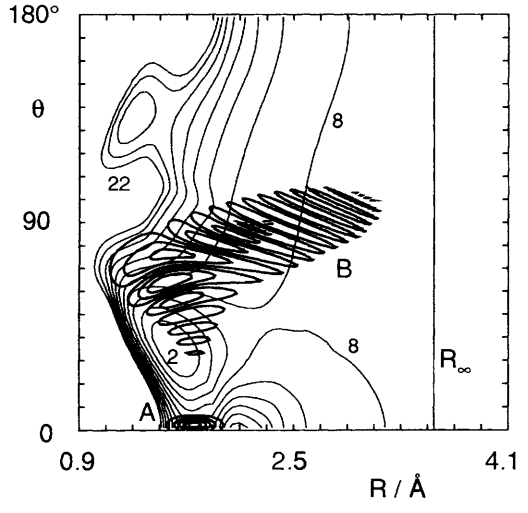

Figure 9 The time-evolution of a wavepacket component on the *ab initio* ground-state potential energy surface of HCO. R and θ are Jacobi coordinates for H relative to CO. A; a component appropriate to crossing from the linear excited state: B; the real part of this wavepacket component 15.9fs later. The asymptotic analysis of the wavepacket to give CO level populations is carried out at R_∞. The energy interval between potential contours is 2000 cm^{-1}; three contours are labelled with the values of $V/1000\,cm^{-1}$.

Fourier analysis of this outgoing wave leads to predicated CO level populations as a function of the HCO energy. Figure 10 presents this analysis for excitation of HCO at 14908 cm^{-1}.[8] This predicts the greatest vibrational population of CO to be for $v_{CO} = 0$, but with extensive rotational excitation peaking between $J(CO) = 35$ and 40. This is in good agreement with experimental measurements following photolysis through a number of HCO* states in this general energy range. One aspect of this population distribution is that less than half of the available energy is released as internal energy of the CO product. This arises because the angular momentum composition of the outgoing wavepacket is established at quite short range, where much of the energy is locked up in centrifugal motion which evolves to become product recoil.

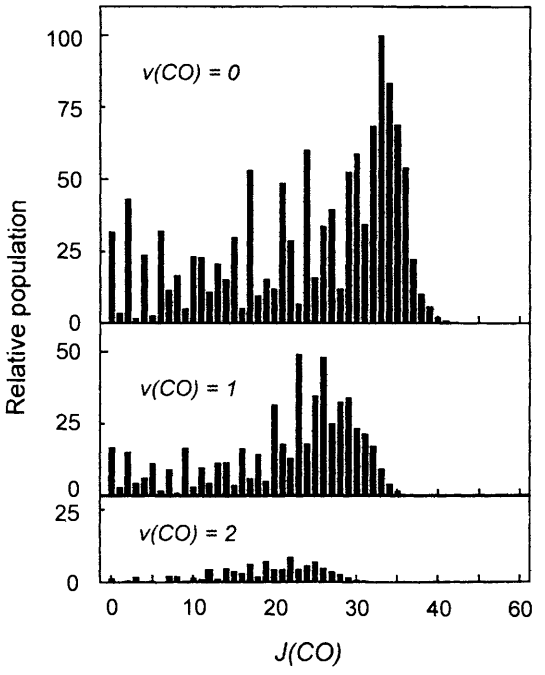

Figure 10 Calculated CO vibration–rotation product distribution following dissociation of HCO through the (0,0,15) vibrational resonance in the $\tilde{A}^2A''$ state at 14908 cm^{-1}.

3.2 The $\tilde{A}^1A_2''$ State of NH_3

This next example involves a vibronic rather than a Coriolis coupling mechanism. Whereas ammonia is pyramidal in its ground state, it is planar in its known excited states, all of which are sufficiently long-lived to show at least vibrational structure. The first excited $\tilde{A}^1A_2''$ state correlates adiabatically over a small potential barrier with the ground-state products $H + NH_2(\tilde{X}^2B_1)$ for motion along a planar dissociation path. It might therefore have been anticipated that excitation to this planar state, reached in the region of 200 nm, would result in most of the energy being released in translational recoil following dissociation on this single surface. However, early attempts to study the energy disposal following the photodissociation of ammonia were frustrated by an inability to assign the spectra of the transient product (presumed to be NH_2), recorded either in emission or by LIF, because of congestion and the ubiquity of unknown spectral lines. The breakthrough came with the development of a method of recording H-atom time-of-flight spectra with high resolution and sensitivity.[12] TOF spectra of the nascent H-atoms from monochromatic photolysis of NH_3 (or D atoms from ND_3) show many sharp peaks, each of which correlates through energy conservation with an internal energy level of the partner NH_2 (or ND_3), (see equation 2).

Excitation to the zero-point level of the $\tilde{A}$-state near 216 nm gives the simplest TOF spectrum, most of the intensity being concentrated into a single series of peaks spanning the full range of the available energy of 1.08 eV (Figure 11). Analysis of this spectrum, with the aid of a calculated energy level manifold for NH_2 ($\tilde{X}^2B_1$), reveals that this series corresponds to rotational excitation concentrated about an axis parallel to H···H, the a-inertial axis, with $N = K_a$. Photolysis at shorter wavelengths proceeds *via* discrete vibrational levels of NH_3 in which the out-of-plane vibration v_2' is excited. The trend is for strong population inversion of the NH_2 states as v_2' (NH_3) is increased, accompanied by a lowering of the average recoil energy of the two partners. The NH_2 motion remains concentrated in a-axis rotation, but there is also some excitation of levels with $N = K_a + 1$ and an increasing excitation of the NH_2 bending

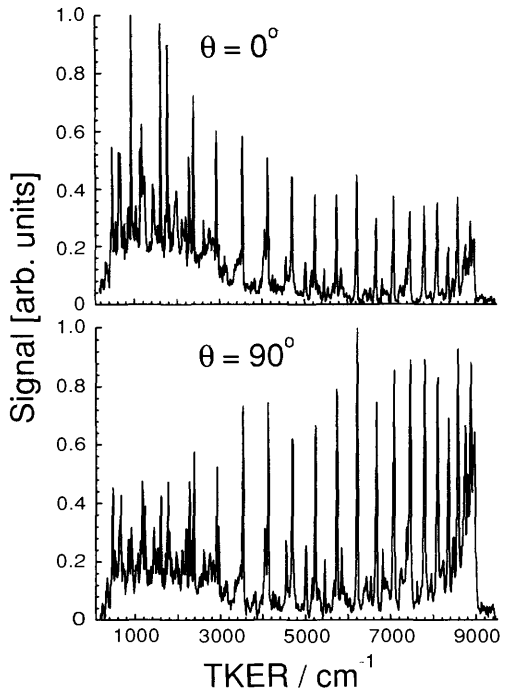

Figure 11 Spectra of the total kinetic energy release (TKER) recorded with H atoms from photolysis of NH_3 in its $\tilde{A}$–$\tilde{X}$ 0_0^0 band at 46197 cm^{-1}. The spectrum recorded with recoil parallel to ϵ_p ($\theta = 0$) is biased towards low recoil velocities and high NH_2 angular momentum; whereas that perpendicular to ϵ_p ($\theta = 90$) is biased towards high velocities and low NH_2 angular momentum.

vibration (Figure 12). In addition to this general trend there is an alternation of internal energy pattern as v_2' increases from 0 to 3.[13]

The interpretation of these observations has been greatly aided by the results of model dynamical calculations on *ab initio* potential energy surfaces. These highlight four aspects of the dissociation mechanism. For $v_2' = 0$ or 1 dissociation can only proceed by quantum tunnelling through a barrier along any one of the NH stretching coordinates, the rates being an order of magnitude slower for ND_3 than for NH_3. A symmetry constraint for non-rotating ammonia requires two quanta of ν_2' for conversion to one quantum of bond stretching, and for $v_2' \geq 2$ dissociation is initiated by such a vibrational redistribution. Thus dissociation from $v_2' = 2$ is mediated *via* anharmonic V–V transfer to the stretching continuum associated with $v_2' = 0$, and $v_2' = 3$ *via* $v_2' = 1$, as clearly demonstrated by comparisons between the product distributions for nv_2' excitation. There is also some evidence that vibration–rotation Coriolis coupling between bending and stretching can give an additional rotational enhancement of dissociation mediated *via* $\Delta v_2' = -1$.[14]

Figure 12 Assignment of the NH_2 internal energy spectrum from photolysis of NH_3 in its $\tilde{A}$–$\tilde{X}$ 2_0^1 band at 47110 cm^{-1}, with detection of H atoms perpendicular to ϵ_p.

However, for all values of v_2' of NH_3, the final dissociation step to ground state H + NH_2 involves a dynamical interaction between motion on the first excited state and on the lowest surface. The dominant feature of this step is that the $\tilde{A}$ and $\tilde{X}$ surfaces exhibit a conical intersection in each H–NH_2 exit channel for planar ammonia (Figure 13). The $\tilde{A}$ surface therefore correlates with *excited state* products for *non-planar* geometries, but this excited state dissociation channel is closed energetically from the lower v_2' levels of excited NH_3. Internal conversion between these states can only proceed by funnelling of trajectories originating in non-planar configurations through these conical intersections, where strong forces amplify the initial inversion motion to generate the high *a*-axis rotation of the NH_2 product. The final energy disposal is therefore very dependent on the value of v_2' (NH_3), and is strongly influenced by the precise geometry and forces acting in the vicinity of this transition structure.

The observed polarization dependence of the TOF spectra (Figure 11) has revealed a striking aspect of the dissociation dynamics. Many of the departing H atoms follow trajectories lying close to the original plane of the excited molecule (*i.e.* perpendicular to ϵ_p). However, where the NH_2 molecule is left in certain very high angular momentum states the H atom follows a path more nearly perpendicular to this plane (*i.e.* parallel to ϵ_p). The exact path followed appears to result from a subtle interplay

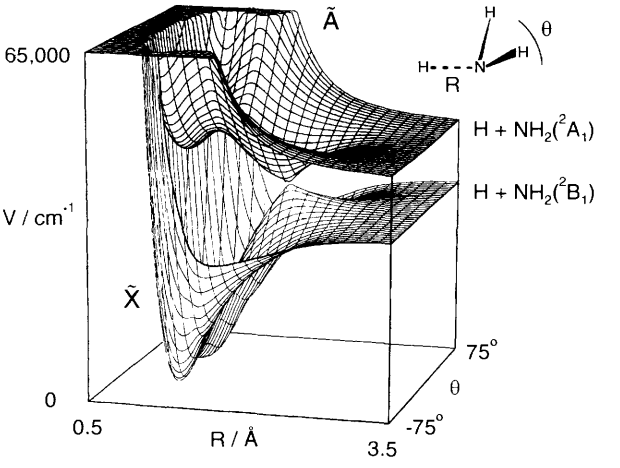

Figure 13 The dependence of the potential energy surfaces for the $\tilde{A}$ and $\tilde{X}$ states of NH_3 on R(H–NH_2) and the out-of-plane angle θ, showing their conical intersection. θ is proportional to the inversion coordinate q_2 for short R, whereas when $R \rightarrow \infty$ it becomes the *a*-axis azimuthal angle of the NH_2 fragment.

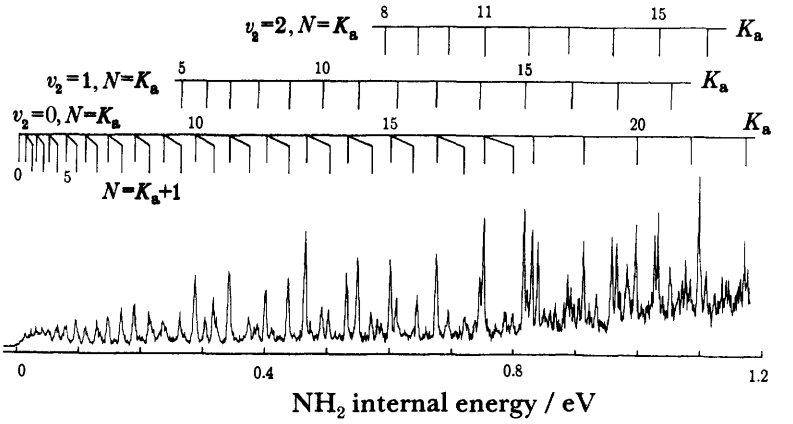

between angular momentum constraints, the heights of centrifugal barriers and the impact distance at which the H atom breaks free

3.3 The $\tilde{B}^1A_1$ State of H_2O

The second excited ($\tilde{B}^1A_1$) state of H_2O, reached near 120 nm, has many features in common with the $\tilde{A}$ state of ammonia Again there is a conical intersection of the excited- and ground-state potential energy surfaces in each exit channel leading to H + OH But in addition there is also a seam of intersection between the surfaces for the $\tilde{B}^1A_1$ and $\tilde{A}^1B_1$ states which comprise a single $^1\Pi_u$ state for linear H_2O These surface crossings are both associated with strong angular forces controlling the dissociation dynamics which are therefore subject to both vibronic and Coriolis coupling mechanisms in this case

Earlier studies of the photodissociation of water vapour at room temperature, recording either the fluorescence of nascent excited OH($A^2\Sigma^+$) or LIF detection of ground state OH($X^2\Pi$), suggested that the Renner–Teller (Coriolis) mechanism through the linear $^1\Pi_u$ intersection provided the major exit route from the $\tilde{B}^1A_1$ state Unfortunately, an energy-dependent predissociation in the A state of OH restricts the range of OH levels that can be monitored in these ways More recently, the Rydberg H-atom TOF technique has facilitated the observation of the full OH product population distribution (Figure 14) [15,16] The H-atom yields through each of the available channels following photolysis at 121 6 nm are given in Table 4 The OH A-state rotational population distribution agrees closely with that derived from spontaneous fluorescence It is strongly inverted peaking at $N' = 20$, which is close to the energetic limit The major ground-state population is even more inverted, peaking at $N'' = 45$ [$N'' = 63$ for OD from D_2O], although this is well below the energetic limit of $N'' = 60$ [$N'' = 83$ for OD] Since the $\tilde{A}$ and $\tilde{X}$ surfaces of H_2O both correlate with H + OH(X), and the OH Λ-doublet splittings are not resolved, this result does not in the first instance allow differentiation between the Renner–Teller ($\tilde{B}^1A_1 \rightarrow \tilde{A}^1B_1$) and conical intersection ($\tilde{B}^1A_1 \rightarrow \tilde{X}^1A_1$) mechanisms

Even so, a striking feature of this OH(X) population distribution is that it exhibits a significant shoulder at $N'' = 40$ (even more marked near $N'' = 50$ for OD from D_2O, Figure 15) The interpretation of these distributions has been greatly aided by comparison with theoretical calculations using a time-dependent wavepacket study of the dissociation dynamics, using two-dimensional potential energy surfaces derived from *ab initio* calculations (*i e* with one fixed bond-length) [16] These show that for final dissociation on the $\tilde{A}$-state surface the product rotation

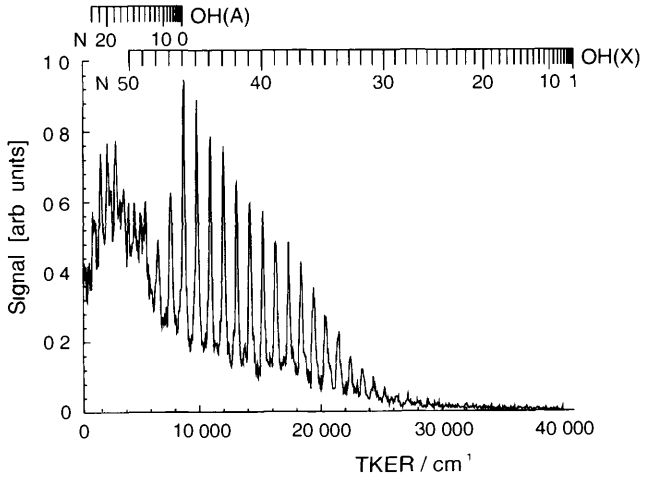

Figure 14 Total kinetic energy spectrum of the fragments recorded with H atoms from photolysis of jet-cooled H_2O at 121 6 nm The OH(X) and OH(A) internal energy scales are taken from the literature

Table 4 H-atom yields through the available channels for dissociation of $H_2O(D_2O)$ at 121 6 nm

Channel	H_2O	D_2O
H/D + OH/OD(X)	64%	62%
H/D + OH/OD(A)	14%	30%
H/D + H/D + O(^{3}P)	22%	8%

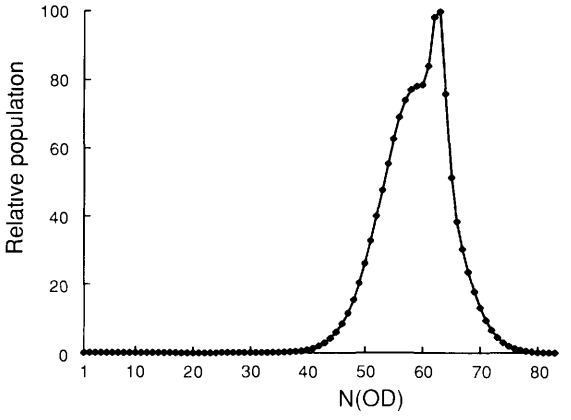

Figure 15 Experimentally derived rotational state population distribution in the OD (X, $v = 0$) fragments arising from 121 6 nm photodissociation of D_2O

is entirely generated on the $\tilde{B}$ surface while the H_2O molecule is opening out towards linearity and one bond is stretching (Figure 16a), the $\tilde{A}$ surface has no angular anisotropy at long range (Figure 16c) In contrast, for final dissociation on the $\tilde{X}$ surface the rotation gained *via* motion on the $\tilde{B}$ surface is augmented by further angular acceleration arising from the anisotropy of the conical feature on the $\tilde{X}$ surface (Figure 16b) In either case a centrifugal barrier prevents the population of the highest OH levels which are energetically accessible at infinite separation of H from OH The overall population distribution for OH(X) is therefore the sum of two components, one peaking at a higher value of N'' than the other Since the Coriolis mechanism depends on rotation of the parent molecule, the relative contributions of these two components will be proportional to the expectation value of $\langle K_a^2 \rangle$ for the excited H_2O ($\tilde{B}^1A_1$) molecules, and will therefore vary with the temperature of the H_2O sample

On this basis it has been concluded that at the beam temperature of *ca* 100—150 K used for the TOF experiment (at which the value of $\langle K_a^2 \rangle \approx 2\,5$ for H_2O^* and 3 7 for D_2O^*) the $\tilde{B} \rightarrow \tilde{A}$ electronic Coriolis coupling makes a significant contribution to the overall dissociation [most obviously manifest by the shoulder near $N'' = 50$ in the OD(X) product rotational distribution, Figure 15], but that the $\tilde{B} \rightarrow \tilde{X}$ vibronic coupling mechanism dominates Lowering the temperature of a thermal beam would lower the range of K_a values excited, $\langle K_a^2 - 1 \rangle$ being approximately proportional to the absolute temperature Thus at a low enough temperature the Coriolis coupling would almost cease to operate, and the dissociation to give ground-state OH would proceed almost entirely *via* the $\tilde{B} \rightarrow \tilde{X}$ route and lead only to the Λ-doublets of e,A′ symmetry

4 Dissociation by Internal Conversion

The examples of photodissociation discussed above have the common feature that the product population distribution is dynamically controlled, with only a sub-set of the molecular degrees of freedom implicated in the dynamics This will tend to be the case where the surfaces are such that classical trajectories issuing from the Franck–Condon region cluster on an excited-

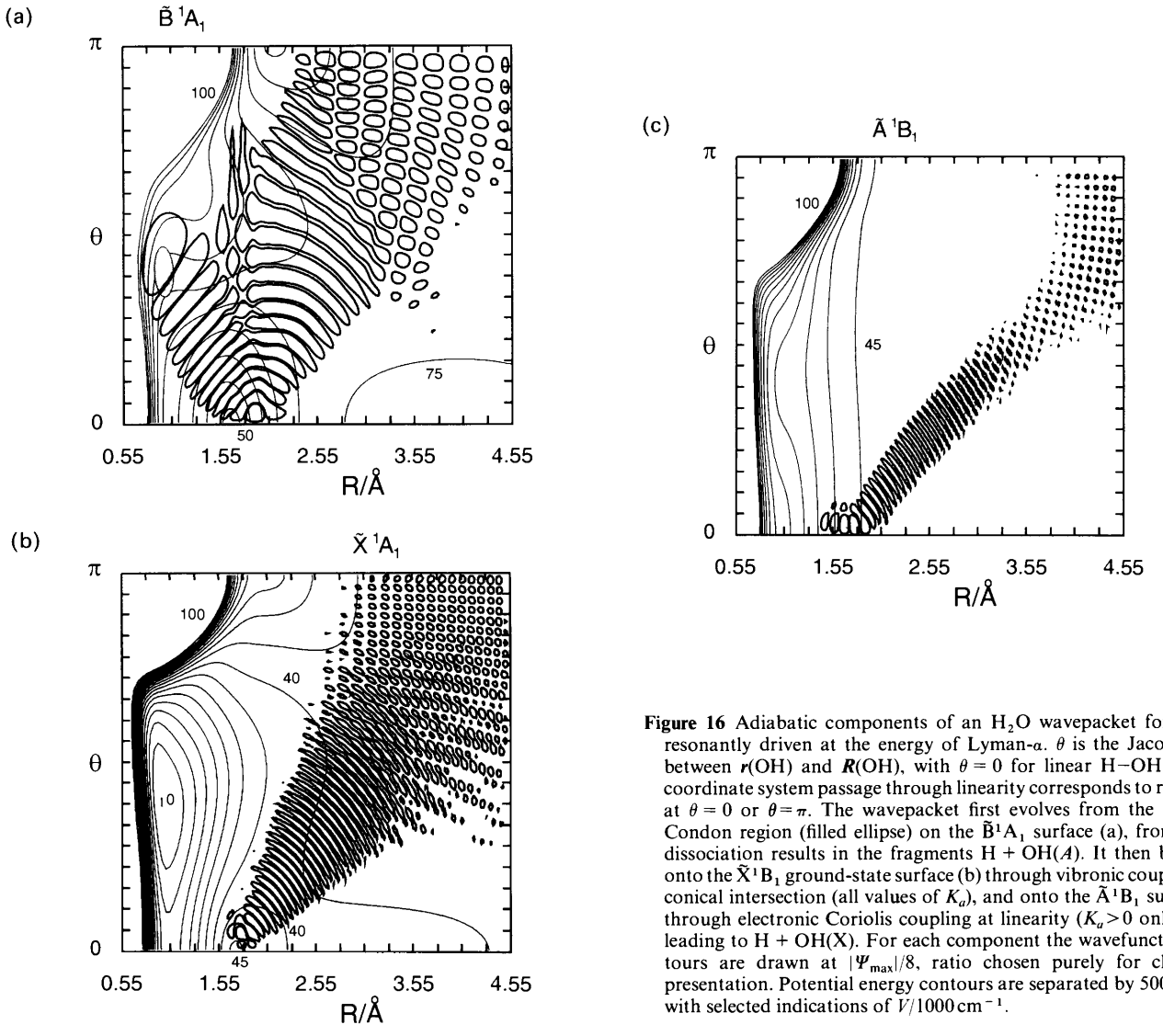

Figure 16 Adiabatic components of an H_2O wavepacket for $K_a = 2$ resonantly driven at the energy of Lyman-α. θ is the Jacobi angle between r(OH) and R(OH), with $\theta = 0$ for linear H–OH. In this coordinate system passage through linearity corresponds to reflection at $\theta = 0$ or $\theta = \pi$. The wavepacket first evolves from the Franck–Condon region (filled ellipse) on the $\tilde{B}^1A_1$ surface (a), from which dissociation results in the fragments H + OH(A). It then branches onto the $\tilde{X}^1B_1$ ground-state surface (b) through vibronic coupling at a conical intersection (all values of K_a), and onto the $\tilde{A}^1B_1$ surface (c) through electronic Coriolis coupling at linearity ($K_a > 0$ only), both leading to H + OH(X). For each component the wavefunction contours are drawn at $|\Psi_{max}|/8$, ratio chosen purely for clarity of presentation. Potential energy contours are separated by 5000 cm^{-1}, with selected indications of $V/1000\,cm^{-1}$.

state surface as they move out to dissociation, even when this motion involves a surface crossing.

However, the concept of nuclear motion on potential energy surfaces is based on the Born–Oppenheimer approximation that nuclei are infinitely heavier than electrons, and thus move independently. All excited states are embedded in the upper reaches of the molecular ground-state and of any other lower states, and even a weak electron–nuclear coupling may mix levels of similar energies in different electronic states. In consequence, in large molecules with high level densities the excited states usually exhibit a rapid decay by internal conversion to the ground state, or inter-system crossing to a manifold of states of different spin multiplicity (*e.g.* triplet states), even though there may be no surface crossings to provide a direct pathway between the states. These decay routes can be expected to play an important role in any photochemistry by opening an indirect path to dissociation on a lower electronic surface, resulting in an energy disposal in the photo-products which may tend to be statistically rather than dynamically controlled.

4.1 The $\tilde{A}^1A''$ State of HNO

Many of the levels of the $\tilde{A}$ state of HNO are long-lived, with a radiative lifetime of *ca.*25 μs. The LIF excitation spectrum is highly structured, but exhibits a breaking-off in the band structure for all excited levels which lie above ~ 16450 cm^{-1}, except for a few levels with $J' = 0$. Direct dissociation on the excited surface at this energy is hindered by a substantial potential barrier, but predissociation nevertheless occurs to $H(^2S) + NO(X^2\Pi)$. Below this limit there are numerous small rotational perturbations. In this example the levels with $J' = 0$ have odd parity to inversion, and cannot mix with $J'' = 0$ levels of the $\tilde{X}^1A'$ ground state which have even parity. Internal conversion is therefore forbidden at any energy for such levels. However, for each value of J greater than 0 there are levels of both parities in each state, so that there is no such strict symmetry constraint in the rotating molecule. Dissociation *via* internal conversion is promoted through an electronic Coriolis mechanism, and Figure 17 shows how the fluorescence quantum yield falls with increasing J-value in the 101–000 vibronic band.[17] The observed fluorescence breaking-off limit for $J' > 0$ is the dissociation energy on the *ground state* surface, with J as the only controlling quantum number. The perturbations in the structured part of the spectrum arise through this same interaction mechanism.

The dissociation products of HNO have not yet been characterized, but this same chromophore is present in all nitroso compounds. Larger RNO molecules have torsional vibrations in which some of the atoms move perpendicular to the CNO local plane of symmetry. These vibrations play the same role as does rotation in HNO in promoting internal conversion from the $\tilde{A}$ to the $\tilde{X}$ state, but for all values of J' including zero. Consequently all levels above the dissociation threshold lead to very rapid fragmentation and complete loss of fluorescence. NCNO disso-

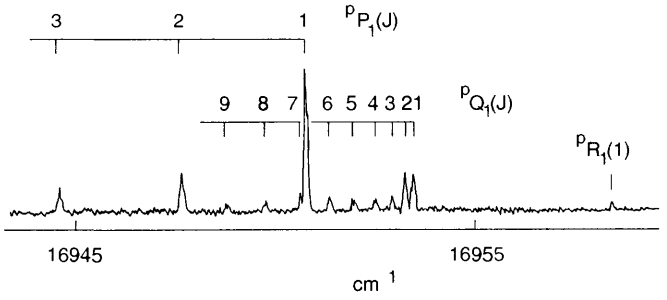

Figure 17 The laser-induced fluorescence excitation spectrum of ambient temperature HNO in a band lying above the dissociation threshold to H + NO The rapid drop in intensity with increase in J' is a consequence of rotationally induced internal conversion to the continuum of the ground state, followed by dissociation ($^{P}P_{1}(1)$ is the only transition that terminates on $J' = 0$)

ciation has been studied in detail, with particular attention to energies near the dissociation threshold This provides a good example of a statistical rotational energy disposal in the dissociation products, although when a vibrational channel becomes open at higher energy the product vibration is not statistically equilibrated with rotation [18]

4.2 The $\tilde{A}^1T_2$ State of CH_4

In contrast to HNO, the first excited state of methane is orbitally degenerate The photodissociation of methane at 121 6 nm has been studied using the technique of H-atom photofragment translational spectroscopy [19] It was concluded from the analysis of the TOF spectrum that simple C–H bond fission is the dominant primary process at this energy The resulting CH_3 fragments are formed with very high levels of internal excitation, such that some 25% possess so much energy that they undergo subsequent unimolecular decay The experiments do not provide a unique determination of this secondary decay process, but arguments based on unimolecular rate theory suggest that predominantly it will yield CH and H_2 fragments

The energy dependence of the TOF spectrum up to the onset of the $CH_3^{\ddagger}$ unimolecular decay can be simulated with a statistical model which uses the density of states for the six (anharmonic) vibrational modes of CH_3, but ignoring rotation (Figure 18) Above the dissociation limit for $CH_3^{\ddagger} \rightarrow CH + H_2$ the secondary decay rate estimated using RRKM theory rises

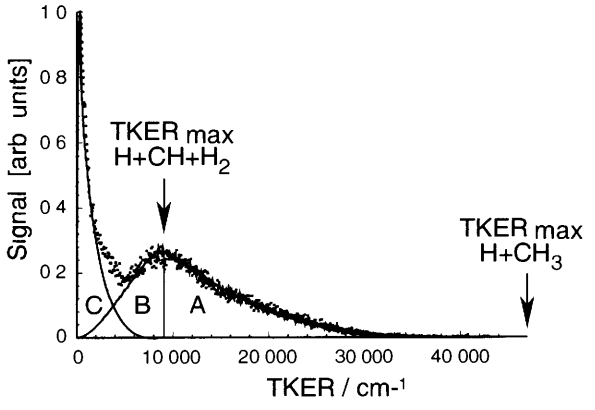

Figure 18 The spectrum of total kinetic energy release (•••) recorded with H atoms from photolysis of CH_4 at 121 6 nm, and its statistical simulation (——) Area A is the calculated vibrational density of states for CH_3 from $CH_4 \rightarrow H + CH_3$ up to the dissociation limit $D_0(CH–H_2)$ Above this limit (area B) rapid dissociation of $CH_3^{\ddagger}$ limits the available density of states Area C is attributed to direct three body dissociation into H + CH + H_2

very rapidly It has then been assumed that departure of the TOF profile from the predictions of the H + CH_3 statistical model comes about because simultaneous dissociation of CH_4^{*} into H + CH + H_2 takes over from the sequential dissociation, leading to a modification of the relevant density of states

It is interesting to enquire as to why this dissociation of methane is essentially statistical, whereas that discussed above for ammonia is dynamically controlled An important difference is that the $^1T_2$ excited electronic state of CH_4 probably suffers from substantial Jahn–Teller distortion Furthermore, both of the triply degenerate vibrational modes ν_3 and ν_4 are of appropriate symmetry not only to induce Jahn–Teller distortion of the excited state, but also to promote vibronic coupling between the excited state and the ground state We do not believe that the good agreement with the results of a statistical calculation necessarily implies that the time scale of the CH_4 dissociation is sufficiently long for complete randomization of all modes in the photoexcited molecule, but rather that the strong Jahn–Teller distortions and vibronic couplings that occur whilst the molecule evolves from the Franck–Condon region of the excited state into the H + CH_3 exit channel of the ground state lead to population of a very wide spread of product vibrational states

5 Discussion

The molecular systems discussed above have been chosen to illustrate the variety of dissociation mechanisms and energy disposal in small polyatomic molecules An important question that follows is whether we are yet in a position to predict the likely outcome of any given photodissociation process In favourable cases the relevant potential energy surfaces may be available from *ab initio* calculation or semi-empirical modelling Alternatively, prediction may be based on analogies with well-studied systems Whether dissociation will take place on one, or more than one, surface will depend critically on both the energies and associated internal coordinates of any surface crossings, on the strengths of their associated inter-state couplings, and on the Frank–Condon region of coordinates from the initial state

For example, in H_2S there is a conical intersection of the first two excited surfaces close to the Frank–Condon region for excitation from the ground state With stretching of either bond one of these surfaces correlates smoothly with the known ground state products H + SH (or HS + H) If, however, one H atom is substituted by a methyl group the symmetry is lowered, such that the C–S bond strength is substantially lower (3 15 eV) than that of the S–H bond (3 75 eV), and the crossing of the corresponding surfaces is no longer in the Franck–Condon region Dissociation in the wavelength range 275–220 nm *via* the first excited $1^1A''$ state results in fission of the *stronger* S–H bond Shorter wavelengths favour population of the second excited $2^1A''$ state, which is bound with respect to both S–H and C–S bond fission, but has an extended C–S bond length Dissociation *via* this second excited state is believed to involve C–S bond stretching, followed by a crossing to the first excited surface which is unbound with respect to both CH_3S + H and CH_3 + SH at these energies Experiment shows that the latter fragmentation channel becomes increasingly important at excitation wavelengths shorter than 220 nm [20] These, and other related, observations can be rationalized in the light of recently reported *ab initio* surfaces, but would have been hard to predict by simple analogy

In contrast, the potential energy surface for the dissociation of the first excited state of the methyl radical, $CH_3(\tilde{B}^2A_1) \rightarrow H + CH_2(\tilde{A}^1A_1)$, must be crossed at long range in its exit channel by the surface for $CH_3(\tilde{X}^2B_1) \rightarrow H + CH_2(\tilde{X}^3B_1)$, with the possibility of coupling through vibronic or Coriolis forces as in ammonia [21] Even so, the adiabatic route is found to be dominant, so the coupling is presumably too weak to be effective [22] (An earlier contradictory observation[21] was incorrectly interpreted)

A second aspect concerns the observation that a statistical population distribution in the products is a characteristic of

dissociation *via* internal conversion, especially with increasing molecular size But consider now the dissociation of deuterated ammonia molecules With ND_3 the outcome of dissociation through the $\tilde{A}$ state is very similar to that described in Section 3 2 for NH_3, apart from a closer energy spacing because of the increased mass For NHD_2, TOF spectra have been recorded for both H and D atom products, with a branching ratio of about 5 1 The H-atom TOF spectrum again shows the simple regular structure associated with *a*-axis rotation of ND_2, but that of the D-atom is densely structured, almost continuous, and unassignable [23] The constrast between one dynamically controlled mechanism, and a second apparently statistically controlled mechanism in competition, indicates that this must be an exit channel effect The most likely explanation is that the torque on the NHD product generated by a breaking N–D bond is perpendicular to that bond, and thereby makes an angle of about 18° to the *a*-axis of NHD The resultant tumbling motion then leads to population of most of the energetically accessible rotational states for this channel only

The size of molecules for which *ab initio* calculations of potential energy surfaces are feasible is increasing rapidly This has already proved its value in a molecule such as CH_3SH, where the number of active coordinates is restricted to the C–S–H backbone However, in general it is at present premature to expect accurate predictions of the dissociation dynamics of most polyatomics in advance of experiment

Photodissociation has often been referred to as a half-collision A full bimolecular reaction can be considered as two such half-collisions back to back with a range of close encounters The experimental and theoretical developments that have been so fruitful in studies of gas-phase photodissociation are now being applied to bimolecular reaction dynamics, and are also finding applications in such fields as the photochemisty of molecules on surfaces

Acknowledgements I am indebted to many gifted graduate students and other collaborators who have contributed to this work, and in particular to my colleagues Professor M N R Ashfold, Drs G G Balint-Kurti and C M Western, and Mr K N Rosser Support from the S E R C for this research is also gratefully acknowledged

6 References

1 G Herzberg, 'Molecular Spectra and Molecular Structure III Electronic Spectra and Electronic Structure of Polyatomic Molecules', Van Nostrand, Princeton, 1966
2 P Andresen, G S Ondrey, B Titze, and E W Rothe, *J Chem Phys*, 1984, **80**, 2548
3 K -H Gericke, S Klee, F J Comes, and R N Dixon, *J Chem Phys*, 1986, **85**, 4463
4 R N Dixon, *J Chem Phys*, 1986, **85**, 1866
5 R Vasudev, R N Zare, and R N Dixon, *J Chem Phys*, 1984, **80**, 4863
6 R N Dixon and H Rieley, *J Chem Phys*, 1989, **91**, 2308
7 R N Dixon, *Trans Faraday Soc*, 1969, **65**, 3141
8 R N Dixon, *J Chem Soc Faraday Trans*, 1992, **88**, 2575
9 R N Dixon, *Mol Phys*, 1985, **54**, 333
10 S H Kable, J -C Loison, D W Neyer, P L Houston, I Burak, and R N Dixon, *J Phys Chem*, 1991, **95**, 8013
11 S H Kable, J -C Loison, P L Houston, and I Burak, *J Phys Chem*, 1990, **92**, 6332
12 J Biesner, L Schnieder, J Schmeer, G Ahlers, Xiaoxiang Xie, K H Welge, M N R Ashfold, and R N Dixon, *J Chem Phys*, 1988, **88**, 3607
13 J Biesner, L Schnieder, G Ahlers, Xiaoxiang Xie, K H Welge, M N R Ashfold, and R N Dixon, *J Chem Phys*, 1989, **91**, 2901
14 M N R Ashfold, R N Dixon, S J Irving, H -M Koeppe,, W Meier, J R Nightingale, L Schnieder, and K H Welge, *Philos Trans Roy Soc London A*, 1990, **332**, 375
15 H J Krautwald, L Schnieder, K H Welge, and M N R Ashfold, *Farad Discuss Chem Soc*, 1986, **82**, 99
16 D H Mordaunt, M N R Ashfold, and R N Dixon, *J Chem Phys*, 1994, **100**, 7360
17 R N Dixon, K B Jones, M Noble, and S Carter, *Mol Phys*, 1981, **42**, 455
18 I Nadler, M Noble, H Reisler, and C Wittig, *J Chem Phys*, 1985, **82**, 2608
19 D H Mordaunt, I R Lambert, G P Morley, M N R Ashfold, R N Dixon, C M Western, L Schnieder, and K H Welge, *J Chem Phys*, 1993, **98**, 2054
20 S H S Wilson, M N R Ashfold, and R N Dixon, *J Chem Phys*, 1994, in press
21 S H S Wilson, M N R Ashfold, and R N Dixon, *Chem Phys Lett*, 1994, **222**, 457
22 S H S Wilson, J D Howe, K N Rosser, M N R Ashfold, and R N Dixon, *Chem Phys Lett*, 1994, **227**, 456
23 D H Mordaunt, Ph D thesis, University of Bristol, 1994, D H Mordaunt, R N Dixon, M N R Ashfold, and L Schneider, in preparation